Contrast dispersion imaging for cancer localization

Massimo Mischi and Hessel Wijkstra

Abstract— **Cancer growth is associated with angiogenic processes in many types of cancer. Several imaging strategies have therefore been developed that target angiogenesis as a marker for cancer localization. To this end, intravascular and extravascular tissue perfusion is typically assessed by dynamic contrast enhanced (DCE) ultrasound (US) and MRI. All the proposed strategies, however, overlook important changes in the microvascular architecture that result from angiogenic processes. To overcome these limitations, we have recently introduced a new imaging strategy that analyzes the intravascular dispersion kinetics of contrast agents spreading through the microvasculature. Contrast dispersion is mainly determined by microvascular multi-path trajectories, reflecting the underlying microvascular architecture. This paper reviews the results obtained for prostate cancer localization by US and MRI dispersion imaging, also presenting the latest new developments and future perspectives.**

I. INTRODUCTION

In the last decades, our knowledge on the physiological processes underlying cancer formation and growth has tremendously expanded. This expansion has also been paralleled by improved imaging technology, exploiting the new available physiological insight to achieve better cancer detection. In this context, the established link between cancer growth and neoangiogenesis has played a fundamental role.

Our knowledge on the function of angiogenesis in cancer growth dates back to the work by Folkman [1]. In order to grow beyond the size of few millimeters, cancer requires the formation of new microvessels carrying nutrients [1], [2]. The resulting microvascular network can therefore be considered as a marker for the presence of those angiogenic processes associated with cancer growth. As a result, angiogenesis imaging has been introduced as a valid option for cancer detection. In particular, diverse imaging strategies have been developed probing different features characterizing the microvasculature associated with cancer [3].

Different from a regular microvascular architecture, consisting of an organized structure of bifurcating microvessels, an angiogenic microvascular architecture is characterized by a disorganized assembly of irregular, fragile, and leaky microvessels, showing irregular branching and arterovenous shunts, as well as a high degree of tortuosity [1], [2], [3].

A number of imaging methods have been designed with the aim of detecting those features characterizing angiogenic microvasculature [3]. Assuming a link between angiogenesis and increased perfusion, most methods are based on the assessment of intravascular perfusion, either by ultrasound (US) Doppler techniques or by contrast-enhanced imaging [4], [5], [6]. When extravascular agents are employed, the focus shifts from intravascular perfusion to tissue perfusion, with the aim of assessing extravascular leakage into the interstitium due to increased microvascular permeability [7]. In general, the link between angiogenesis and perfusion is rather complex. While increased perfusion is expected due to the formation of new microvessels and the presence of arterovenous shunts, this can be counterbalanced by the small irregular size of the formed microvessels, together with an increase in interstitial pressure due to leakage, resulting all together in increased peripheral flow resistance [8].

While perfusion is affected by opposing factors, the microvascular architecture remains a major discriminating factor between benign and malignant tissue. Therefore, we have recently introduced a new imaging approach to characterize the microvascular architecture as a marker for cancer angiogenic processes. Although clinical imaging technology does not permit imaging single microvessels, the proposed method infers the underlying microvascular architecture from the intravascular dispersion kinetics of a contrast agent, estimated by analysis of the agent concentration in time [9] and, more recently, also in space [10].

The proposed method has first been validated for prostate cancer (PCa) localization. In the United States, PCa is the form of cancer with the highest incidence (27%) and second mortality (10%) in men [11]. Despite the availability of effective focal therapies, their timely and efficient use is hampered by a lack of reliable imaging methods for early PCa localization. For the same reason, diagnosis still relies on multiple systematic biopsies.

Prostate imaging in clinical routine is typically performed by US, which is also used for biopsy guidance [12]. However, aiming at PCa localization, in the past years the use of multiparametric (mp)MRI, combining T2, dynamic contrast enhanced (DCE), and diffusion weighted MRI, is gaining attention [13]. DCE-US has also been tested for PCa localization by perfusion quantification [5]. Therefore, we have employed both DCE-US and DCE-MRI for implementing and testing dispersion imaging in the context of PCa localization. These technologies also give the opportunity to evaluate dispersion imaging by use of intravascular (DCE-US) and extravascular (DCE-MRI) contrast agents.

II. METHODOLOGY

A. Intravascular dispersion

The kinetics of an intravascular contrast agent flowing through a microvascular network can be described as a Brow-

This research was funded by ERC StG 280209 and STW VIDI 10769.

M. Mischi and H. Wijkstra are with the Electrical Engineering Dept, Eindhoven University of Technology, the Netherlands.

H. Wijkstra is also with the Urology Dept, Academic Medical Center, University of Amsterdam, the Netherlands.

978-1-4244-7929-0/14/$26.00 ©2014 IEEE

nian process and modeled with the convective dispersion equation [14]. In one dimension, z, the convective dispersion equation is given as

$$\frac{dC_t(z,t)}{dt} = D\frac{d^2C_t(z,t)}{dz^2} - v\frac{dC_t(z,t)}{dz}, \quad (1)$$

with $C_t(z,t)$ being the contrast-agent concentration in tissue at position z and time t, v its velocity, and D the dispersion coefficient. In the microvasculature, the dispersion coefficient D is mainly determined by transit time distribution due to multipath trajectories of the contrast agent through the microvascular network [14], [15]. Therefore, it reflects the microvascular architecture [9].

A solution of Eq. (1), assuming a fast injection of the contrast agent as a bolus, is given by the Local Density Random Walk (LDRW) model [14]. More recently, in order to define a local dispersion parameter, i.e., independent of the history of the contrast bolus between the injection and detection site, a modified version of the LDRW model has been proposed [9]. Its formulation is given as

$$C_t(t) = v_p\alpha\sqrt{\frac{\kappa}{2\pi(t-t_0)}}e^{\frac{-\kappa(t-t_0-\mu)^2}{2(t-t_0)}}. \quad (2)$$

with t_0 being the theoretical injection time (assuming the indicator kinetics to be constant along the entire path between injection and detection site), v_p the fractional plasma volume in the investigated tissue sample (voxel), $v_p\alpha$ the time integral of $C_t(t)$, μ the mean transit time of the indicator between injection and detection site, and κ the estimated intravascular dispersion parameter, $\kappa = v^2/D$, which represents the local ratio between contrast convection (squared velocity v^2) and dispersion (dispersion coefficient D).

Equation (2) is a solution of the convective dispersion equation assuming a Gaussian distribution of the contrast bolus in space prior to its passage through the detection site [9]. It represents the contrast-agent time-concentration curve (TCC) at the detection site; therefore, by fitting Eq. (2) to TCCs measured at each voxel, a map of the dispersion parameter κ can be generated.

B. Contrast ultrasound dispersion imaging

Gas microbubbles stabilized with a biocompatible shell are the employed contrast agents in DCE-US. To validate contrast ultrasound dispersion imaging (CUDI) for PCa detection, a 2.4-mL bolus of SonoVue® (Bracco) contrast agent is injected. Due to their size, comparable to blood red cells, SonoVue® microbubbles flow through the smallest microvessel while staying in the blood pool [16]. Both an iU22 (Philips Healthcare) and a UltraView 800 (BK medical) ultrasound scanner were employed for the measurement in contrast-specific imaging at low mechanical index. Contrast-specific imaging exploits the nonlinear microbubble backscatter as compared to that from (linear) tissue in order to enhance specific microbubble detection [17]. Assessment of absolute TCCs by DCE-US is usually unfeasible, and time-intensity curves (TICs) recorded at each pixel are employed for the following dispersion analysis after linearization [18].

A first option consists of fitting Eq. (2) to the measured (linearized) TICs in order to generate a map of the dispersion parameter κ [9]. Unfortunately, due to the poor signal-to-noise ratio (SNR) in measured TICs and the presence of recirculation, model fitting remains a critical procedure that is time demanding and prone to errors. An alternative approach was therefore proposed that provides an indirect estimation of dispersion by full spatiotemporal analysis [10]. This approach was originally based on the intuition that low dispersion results in neighbor TICs showing higher similarity with each other. To the limit, in the absence of dispersion, neighbor TICs would result identical.

Implementation of the similarity analysis requires the definition of both a strategy for TIC comparison and a similarity measure. Each TIC was compared with the neighbor TICs measured from an annular ring whose size provided the best balance between diagnostic resolution and robustness to noise, while also accounting for the scanner resolution [10]. The first similarity measure, referred to as coherence, ρ, consisted of the correlation coefficient of the TIC amplitude spectra in a frequency range representative of the contrast kinetics [10]. By neglecting the phase information, the TIC arrival time cannot alter the TIC shape similarity. Later on, time windowing and speckle regularization was introduced to focus on the most informative TIC time interval and to prevent anisotropic, depth-dependent speckle size from influencing the spatiotemporal analysis [19].

Based on the implemented time-windowing strategy, detection of the TIC appearance time was also available and could be used to realign the measured TICs prior to the similarity analysis. This way, the phase information could be added to the similarity measure without being affected by TIC appearance time. The correlation coefficient, r, of the realigned TICs was therefore introduced as new similarity measure [20]. Moreover, an analytical link between the dispersion parameter κ and the correlation coefficient r could be established, evidencing a monotonic relation and providing a solid analytical and physical basis for the proposed similarity analysis [20].

Given the link between linear similarity measures, such as coherence and correlation, and dispersion kinetics, the statistical dependency between neighbor TICs, accounting for nonlinear similarity, was also investigated. In particular, the mutual information between IDCs was explored as a possible similarity measure [21]. Like for linear similarity, also mutual information is estimated between a central pixel and its neighbors within a predefined kernel [21]. Time windowing was also implemented to extract the contrast washin phase, showing higher SNR and stationarity.

C. Magnetic resonance dispersion imaging

Assessment of intravascular dispersion by CUDI is facilitated by the use of intravascular agents. Instead, when using DCE MRI, the adopted gadolinium-based contrast agents are made of small molecules that leak outside the blood

pool into the extravascular extracellular space (interstitium), complicating the assessment of the intravascular dispersion. New dispersion models are therefore needed that take extravasation into account.

MRI acquisition consisted of a multislice spoiled gradient recalled sequence following the intravenous injection of a 0.1-mmol/Kg bolus of Gadovist® (Bayer). All scans were performed with a 1.5-T MRI scanner (Magnetom Avanto, Siemens) and an endorectal coil. Voxel size and time resolution were 1.67x1.67x4 mm^3 and 3.1 ms, respectively; this spatiotemporal resolution is considerably inferior to that by DCE-US. Pre-contrast T1 maps were estimated by an inversion recovery sequence to obtain the absolute contrast concentration according to [22], yielding an absolute TCC for each voxel.

For an extravascular agent, the measured concentration in tissue, $C_t(t)$, results from the contribution of the intravascular concentration in blood plasma, $C_p(t)$, and the extravascular concentration in the interstitium, $C_e(t)$, given as

$$C_t(t) = v_p C_p(t) + v_e C_e(t), \tag{3}$$

with v_e being the extravascular fractional volume. Based on the established compartmental Tofts model [7], assuming the interstitium to be represented by a single compartment and the contribution of $C_p(t)$ to $C_t(t)$ to be negligible ($v_p \ll v_e$), the extravasation kinetics can be represented as

$$C_t(t) = K^{trans} C_p(t) * e^{-k_{ep}t}, \tag{4}$$

with * convolution symbol, and with K^{trans} and $k_{ep} = K^{trans}/v_e$ representing the volume transfer constant and the back flow rate, respectively [7]. Both K^{trans} and k_{ep} are commonly used as indicators of vascular leakage; however, their estimation requires the intravascular concentration, $C_p(t)$, to be known. $C_p(t)$ is typically estimated by measuring a so called arterial input function (AIF) from the closest artery feeding the investigated tissue. This tedious operation is prone to errors due to inaccurate quantification and modeling, assuming instantaneous mixing of the AIF in the intravascular compartment.

Based on Eq. (1), the intravascular plasma concentration can be modeled by Eq. (2). Therefore, under the assumption of a slow extravascular kinetics as compared to the intravascular kinetics (adiabatic assumption [23]), $C_p(t)$ in Eq. (4) can be represented by the model in Eq. (2), yielding the following dispersion model for extravascular agents [24]

$$C_t(t) = \alpha K^{trans} \sqrt{\frac{\kappa}{2\pi (t-t_0)}} e^{\frac{-\kappa(t-t_0-\mu)^2}{2(t-t_0)}} * e^{-k_{ep}t}. \tag{5}$$

Fitting Eq. (5) to TCCs measured at each voxel permits the simultaneous estimation of a dispersion map, expressed by κ, and a leakage map, expressed by k_{ep}. Focusing on the estimation of the novel parameter κ, this method is referred to as magnetic resonance dispersion imaging (MRDI). K^{trans} cannot be estimated due to its multiplication by the scaling factor α.

D. Validation

Due to the limits of available imaging methods for PCa localization, the only reference for validation consists of the histology results after radical prostatectomy. Slices of 4-mm thickness were marked by the pathologist for the presence of cancer. A number of pilot studies was carried out where patients referred for radical prostatectomy were first analyzed by either CUDI, or MRDI, or both. Validation was then performed by overlaying two regions on the resulting parametric maps that represented, according to the corresponding histology slice, benign and malignant tissue, respectively. Voxel classification for PCa detection was then evaluated in terms of area under the resulting Receiver Operating Characteristic (ROC) curve, sensitivity, and specificity. The proposed dispersion maps were also compared with standard maps based on perfusion or leakage parameters.

MRDI and CUDI data were collected at the Academic Medical Center University Hospital (Amsterdam, Netherlands). CUDI data were also collected at the Jeroen Bosch Hospital, ('s-Hertogenbosch, Netherlands). All these studies were approved by the local Ethical Boards and written consent was collected from all patients.

III. RESULTS

Table I presents an overview of the available results is terms of sensitivity, specificity and ROC curve area. The most extended CUDI validation consists of a multicenter study comprising 43 measurements in 24 patients examined at the AMC (19) and the Jeroen Bosch Hospital (5) [25]. Both correlation and coherence maps outperformed classification by standard perfusion parameters by over 10% in sensitivity, specificity, and ROC curve area. Due to poor SNR and unreliable fitting, dispersion maps by the parameter κ are less accurate [20]. Instead, nonlinear similarity maps by mutual information , I, show promising results based on a first pilot study with 9 patients scanned at the AMC University Hospital [21]. MRDI has successfully been validated with 15 patients [24]. Again, classification by the proposed dispersion map outperformed that by standard leakage parameters k_{ep} and K^{trans} by over 10%.

TABLE I
CLASSIFICATION RESULTS.

Dispersion parameter	Sens (%)	Spec (%)	ROC
r (43 CUDI planes, 24 patients [25])	77.9	82.4	0.88
ρ (same dataset as above*)	77.3	81.3	0.87
κ (12 CUDI planes, 8 patients [20])	66.6	68.7	0.70
I (21 CUDI planes, 9 patients [21])	81	87	0.92
κ (90 MRDI slices, 15 patients [24])	85.0	90.2	0.94

* Unpublished results.

Fig. 1 shows the same prostate investigated by CUDI and MRDI, and compared with the corresponding histology. Approximately corresponding US, MRI, and histology planes/slices are shown. The estimated κ values by CUDI and MRDI are 0.37 ± 0.08 s^{-1} (1193 pixels) and 0.05 ± 0.01 s^{-1} (26 voxels) for benign tissue and 0.68 ± 0.10 s^{-1} (1115 pixels) and 1.01 ± 0.77 s^{-1} (21 voxels) for malignant tissue.

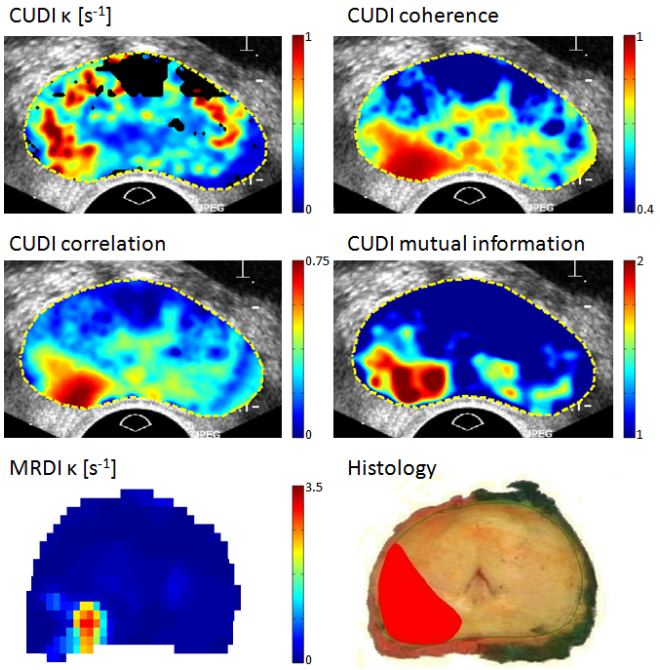

Fig. 1. Parametric dispersion maps by CUDI and MRDI based on different methods with corresponding histology result. Red color represents cancer.

IV. DISCUSSION AND CONCLUSIONS

Dispersion imaging has recently been proposed as a new promising option for imaging angiogenesis and, therefore, for cancer localization. Here the progress with CUDI and MRDI for PCa localization is reported and evaluated. The results confirm the potential of these methods, although validation with larger datasets is necessary prior to clinical adoption.

DCE US, making use of intravascular agents, facilitates the implementation of the method by simpler models. On the other hand, DCE MRI, making use of extravascular agents, permits the simultaneous assessment of the two main markers for cancer microvasculature: microvascular leakage and architecture.

Results by CUDI and MRDI are proposed for the first time in the same patient. The obtained dispersion values are in line, with the dispersion parameter $\kappa = v^2/D$ increasing in the presence of cancer. This result, confirmed in all studies, can be explained by an increase in tortuosity, effectively limiting the dispersion kinetics represented by the dispersion coefficient D.

All techniques have so far been validated for PCa localization vs. the corresponding histological results. However, while the histology evaluates the cellular differentiation, dispersion imaging characterizes the microvascular architecture, whose ground truth should be produced by immunohistological analysis. A preliminary study was proposed in mouse xenograft models showing the ability of CUDI to differentiate between microvascular architectures [26], but more extended validation is necessary to assess the link between the estimated dispersion parameters and the main geometrical features of the microvasculature.

REFERENCES

[1] J. Folkman, "Induction of angiogenesis during transition from hyperplasia to neoplasya," *Nature*, vol. 339, pp. 58–61, 1989.

[2] N. Weidner, P. R. Carroll, *et al*, "Tumor angiogenesis correlates with metastasis in invasive prostate carcinoma," *Am J Pathology*, vol. 143, no. 2, pp. 401–409, 1993.

[3] G. Russo, M. Mischi, *et al*, "Angiogenesis in prostate cancer: onset, progression and imaging," *BJU Int*, vol. 110, pp. 794–808, 2012.

[4] N. Elie, A. Kaliski, *et al*, "Methodology for quantifying interactions between perfusion evaluated by DCE-US and hypoxia throughout tumor growth," *Ultrasound Med Biol*, vol. 33, no. 4, pp. 549–560, 2007.

[5] R. J. Eckersley, J. P. Sedelaar, *et al*, "Quantitative microbubble enhanced transrectal ultrasound as a tool for monitoring hormonal treatment of prostate carcinoma," *Prostate*, vol. 51, pp. 256–267, 2002.

[6] E. Halpern, F. Frauscher, *et al*, "Prostate: high frequency doppler US imaging for cancer detection," *Radiology*, vol. 225, pp. 71–77, 2002.

[7] P. Tofts, G. Brix, *et al*, "Estimating kinetic parameters from dynamic contrast-enhanced T1-weighted MRI of a diffusable tracer: Standardized quantities and symbols," *J Magn Reson Imag*, vol. 10, pp. 223–232, 1999.

[8] D. Cosgrove, "Angiogenesis imaging - ultrasound," *The British Journal of Radiology*, vol. 76, pp. S43–S49, 2003.

[9] M. Kuenen, M. Mischi, and H. Wijkstra, "Contrast ultrasound diffusion imaging for localization of prostate cancer," *IEEE TMI*, vol. 30, pp. 1493–1502, 2011.

[10] M. Mischi, M. Kuenen, and H. Wijkstra, "Angiogenesis imaging by spatiotemporal analysis of ultrasound-contrast-agent dispersion kinetics," *IEEE TUFFC*, vol. 59, no. 4, pp. 621–629, 2012.

[11] American Cancer Society, "Cancer facts & figures 2014," *Atlanta: American Cancer Society*, 2014.

[12] F. Aigner, M. Mitterberger, *et al*, "Status of transrectal ultrasound imaging of the prostate," *J Endourol*, vol. 24, no. 5, pp. 685–691, 2010.

[13] J. Barentsz, J. Richenberg, *et al*, "Esur prostate mr guidelines 2012," *Eur Radiol*, vol. 22, no. 4, pp. 746–757, 2012.

[14] C. W. Sheppard, *Basic principles of the tracer method*. New York: John Wiley and Sons, 1962.

[15] G. I. Taylor, "Dispersion of soluble matter in solvent flowing slowly through a tube," *Proc R Soc Lond*, vol. 219, no. 1137, pp. 186–203, 1953.

[16] J. M. Gorce, M. Arditi, and M. Schneider, "Influence of bubble size distribution on the echogenicity of ultrasound contrast agents: A study of SonoVue^{TM}," *Invest Radiol*, vol. 35, no. 11, pp. 661–671, 2000.

[17] N. de Jong, A. Bouakaz, and F. J. ten Cate, "Contrast harmonic imaging," *Ultrasonics*, vol. 40, pp. 567–573, 2002.

[18] N. G. Rognin, P. J. A. Frinking, *et al*, "In-vivo perfusion quantification by contrast ultrasound: validation of the use of linearized video data vs. raw RF data," in *2008 IEEE IUS*, Beijing, Nov. 2–5 2008, pp. 1690–1693.

[19] M. Kuenen, T. Saidov, *et al*, "Contrast-ultrasound dispersion imaging for prostate cancer localization by improved spatiotemporal similarity analysis," *Ultrasound Med Biol*, vol. 39, no. 9, pp. 1631–1641, 2013.

[20] ——, "Spatiotemporal correlation of ultrasound-contrast-agent dilution curves for angiogenesis localization by dispersion imaging," *IEEE TUFFC*, vol. 60, no. 12, pp. 2665–2669, 2013.

[21] N. Bouhouch, L. Demi, *et al*, "Contrast-enhanced angiogenesis imaging by mutual information analysis," in *19th Eur Symp Ultrasound Contrast Imaging*, Rotterdam, Jan. 23–24 2014, pp. 139–142.

[22] M. Schabel and D. Parker, "Uncertainty and bias in contrast concentration measurements using spoiled gradient echo pulse sequences," *Phys Med Biol*, vol. 53, no. 9, pp. 2345–2373, 2008.

[23] K. S. St Lawrence and T. Y. Lee, "An adiabatic approximation to the tissue homogeneity model for water exchange in the brain: I. theoretical derivation." *J Cerebr Blood F Met*, vol. 18, no. 12, pp. 1365–1377, 1998.

[24] M. Mischi, S. Turco, *et al*, "MR dispersion imaging for localization of angiogenesis and cancer growth," *Invest Radiol*, 2014, Online Preview, doi: 10.1097/RLI.0000000000000056.

[25] M. Mischi, M. Kuenen, *et al*, "Prostate cancer localization by contrast-ultrasound-dispersion imaging: results from a pilot study," in *29th Annual EAU Congress*, Stockholm, Apr. 11–15 2014.

[26] S. Saidov, C. Heneweer, *et al*, "Contrast ultrasound dispersion imaging of different tumor types," in *IEEE IUS*, Dresden, Oct. 8–9 2012, pp. 2149–2152.